

Cr, Co, Pd, Au, and In overlayers on PbS(100): Adatom interactions and interface formation

B. M. Trafas, I. M. Vitomirov, C. M. Aldao, Y. Gao, F. Xu, and J. H. Weaver

Department of Chemical Engineering and Materials Science, University of Minnesota, Minneapolis, Minnesota 55455

D. L. Partin

General Motors Research Laboratories, Warren, Michigan 48090-9055

(Received 13 June 1988)

High-resolution synchrotron-radiation photoemission has been used to investigate Cr-, Co-, Pd-, Au-, and In-adatom depositions at room temperature on cleaved PbS(100) single-crystal surfaces. In general, these adatoms induce disruption of the substrate but the growth morphology and the distribution of the released Pb and S atoms in the overlayer varies a great deal. The deposition of adatoms of Cr, Co, Pd, and Au in small amounts leads to the appearance of a chemically shifted Pd 5*d* core-level component and at high coverage there is substantial Pb segregation to the free surface. Pb segregation is greatest for Cr and diminishes for Co, Pd, and Au. This ordering reflects differences in the amount of substrate disruption (greatest for Cr, least for Au) and the low solubility of Pb in these metals. The S 2*p* core-level results also reveal chemical changes associated with Cr-sulfide formation and the dissolution of S in, and on, the growing metal overlayer (surface segregation is greatest for Pd and Au and least for Cr). In contrast, studies of the In/PbS interface show that In forms clusters, that there is some disruption of the substrate, that S is expelled to the surface, and that Pb is released into the In overlayer.

INTRODUCTION

The formation of metal overlayers on semiconductors presents a variety of challenging theoretical and experimental problems related to the electrical properties, the tendency for reaction and chemical intermixing, and the possibility of forming unique interface-stabilized products.^{1,2} Photoelectron spectroscopy has been one of the more frequently used of the many experimental techniques to investigate these microscopic properties because it has the ability to examine changes in chemical environment with inherently high surface sensitivity.¹

Major advances in understanding interfacial phenomena have come from studies of such prototypical semiconductors as Si, Ge, GaAs, InP, and some of the ternary semiconductors. In contrast, much less is known about interface formation for the IV-VI compound semiconductors and, to our knowledge, there have been no reported photoemission studies of the microscopic interactions that occur at PbS interfaces. (References 3–5 have provided insight into the microscopic properties of several metal overlayers on PbTe.) At the same time, this system offers the opportunity to correlate phenomena observed at III-V and II-VI compound interfaces to those observed for a system with different bonding and crystal structure, particularly adatom-induced disruption and the coverage-dependent distribution of released anions and cations in the growing metal layer.

Lead sulfide is a small-band-gap semiconductor (0.41 eV at 300 K) which crystallizes in the rocksalt structure.^{6,7} As for the other lead chalcogenides, its main technological applications are in infrared optoelectronic devices as detectors and laser sources.^{8–10} The electronic states of PbS reflect strong ionic bonding that is very

different from the sp^3 hybrid character of the covalent diamond and zinc-blende semiconductors. There is also some small covalent bonding due to the overlap of the directional *p* orbitals of Pb with those of S. The valence bands are therefore mostly *p* type in character, with a lower split-off *s*-like band.^{11–18} X-ray and angle-resolved ultraviolet photoemission studies of PbS have revealed the density of electronic states, the details of the energy bands, and the position of the Fermi level at the (100) surface.^{19–22} Reflection high-energy electron diffraction (RHEED) has been used to study growth modes for thick noble-metal overlayers on PbS(111) at both room and elevated temperatures.²³ Studies of interface formation involving PbTe have shown nonabrupt interfaces with out-diffusion of both Pb and Te atoms.^{3–5}

In this paper we present the results of a room-temperature study of interface formation for Cr/PbS(100), Co/PbS(100), Pd/PbS(100), Au/PbS(100), and In/PbS(100). These metals were chosen in order to consider the interfacial properties for systems which were expected to be reactive (Cr), weakly reactive (Co and Pd), and nonreactive (Au). Indium was expected to be unreactive and to grow on the surface via clusters. As such, the results provide a wide range of behavior for comparison with other semiconductor interfaces.

High-resolution core-level and valence-band results indicate that these metals do not produce atomically abrupt interfaces with PbS. Instead, disruption is observed at low coverage for Cr, Co, Pd, and Au with the greatest amount of disruption and tendency for compound formation being observed for Cr and the least for Au. The high-coverage regime is characterized by metal-overlayer formation accompanied by substantial surface segregation for atoms of both Pb and S. Line-shape analysis of

the Pb 5*d* and S 2*p* core-level energy distribution curves (EDC's) taken with markedly different photoelectron mean free paths makes it possible to model the atom distribution and assess chemical reaction.

EXPERIMENTAL

The photoemission experiments were carried out at the Wisconsin Synchrotron Radiation Center using the Aladdin electron storage ring and a Grasshopper Mark II monochromator and beamline. These measurements emphasized core-level line-shape changes and core-level intensity variations as a function of the amount of metal deposited. Photoelectrons were energy analyzed with a double-pass cylindrical mirror analyzer in a vacuum system described in detail elsewhere.²⁴ The tunability of the photon source made it possible to choose photon energies to give equal electron inelastic mean free paths λ for Pb 5*d* and S 2*p* photoelectrons, namely 60 eV for Pb and 204 eV for S in the surface-sensitive mode ($\lambda \sim 4$ Å) and 40 and 175 eV in the bulk-sensitive mode ($\lambda \sim 9$ Å). Monochromator bandwidths and analyzer pass energies were selected to give overall resolution of ~ 200 meV for the Pb 5*d* core levels. The corresponding resolution was ~ 500 meV for the S 2*p* studies. For the valence-band EDC's, the overall resolution was ~ 400 meV.

The PbS crystals were cut to give rectangular bars $2 \times 2 \times 6$ mm³ with the small face parallel to the (100) plane. The samples were cleaved *in situ* at a pressure of $\sim 5 \times 10^{-11}$ Torr. These samples cleave easily, as expected from their rocksalt structure. The quality of the cleaved surface was judged visually and with valence-band and Pb 5*d* core-level spectra. Adatoms of Cr, Co, Pd, Au, and In were evaporated from resistively heated tungsten boats that had been thoroughly degassed so that the pressure was below 3×10^{-10} Torr during evaporation. An Inficon crystal thickness monitor was used to determine the evaporation rates (typically ~ 1 Å/min). The amount of material deposited will be expressed in angstroms in this paper. The conversion factor to substrate-equivalent monolayers (ML) would be 0.74 ML/Å for Cr, 0.80 ML/Å for Co, 0.60 ML/Å for Pd, 0.52 ML/Å for Au, and 0.34 ML/Å for In, assuming the deposition of one adatom per semiconductor atom site on the PbS(100) surface where the planar density is 1.13×10^{15} atoms/cm².

Analysis of the Pb 5*d* and S 2*p* core-level EDC's was done by line-shape decompositions using a nonlinear least-squares minimization subroutine on an IBM RT computer.²⁵ The method involves simultaneous fitting based on a cubic polynomial background function and components introduced to represent the core-level structures. As discussed in Ref. 25, semiconductor core-level line shapes can be represented by Voigt functions which are the convolution of Lorentzian (core-hole lifetime broadening) and Gaussian (instrument and phonon broadening) functions. For atoms in metallic environments, a more accurate representation is the Doniach-Šunjić (DS) line shape because of the asymmetry at higher binding energy due to screening and many-body interactions at the Fermi level.²⁶ In our analysis adjust-

able parameters included the Lorentzian width, branching ratio, spin-orbit splitting, peak intensities, energy positions, Gaussian linewidths, and background parameters.²⁷ We allowed up to two spin-orbit-split doublets, one representing the substrate and the other representing atoms released from the substrate (no evidence was found for a surface-shifted core level for the clean surface). Our fits were obtained by keeping the Lorentzian width, the branching ratio, and the spin-orbit splitting of all the components of a single atomic species fixed for all coverages at the values determined for the cleaved substrate. The Gaussian widths of the adatom-induced features were allowed to vary to account for changes in local bonding. DS line shapes were used to fit the core-level spectra for the Pb species released from the substrate, and typical values of the asymmetry factor ranged from 0.11 to 0.12. In all cases, self-consistency achieved by fitting all of the spectra taken with two different photon energies and for a range of coverages greatly increased our confidence in the line-shape decompositions.

RESULTS AND DISCUSSION

In the following we address the differences and common features observed during the deposition of reactive (Cr), relatively unreactive (Co, Pd), and nonreactive (Au) metal adatoms onto cleaved PbS(100). Our experimental results indicate substantial Pb segregation for Cr, Co, Pd and Au. There is also sulfur segregation for Co, Pd, and Au and an indication of Cr-S compound formation. The deposition of In also induces disruption and S surface segregation, but the released Pb atoms are dissolved in the In overlayer.

In Figs. 1–5 we summarize the surface-sensitive Pb 5*d* and S 2*p* results for Cr/PbS(100), Co/PbS(100), Pd/PbS(100), Au/PbS(100), and In/PbS(100) interfaces taken at $h\nu = 60$ and 204 eV, respectively ($\lambda \sim 4$ Å). In each case, the Pb 5*d* results are shown on the left and those for S 2*p* are shown on the right. The Pb 5*d* energy scale enables us to observe the full spin-orbit-split pair. Spectra that are vertically offset show the effects of metal deposition. These EDC's have been normalized to constant height to emphasize line-shape changes and have been shifted in energy to account for variations in band bending. Representative line-shape decompositions for Au/PbS in Fig. 4 show how the chemical environments change with metal deposition and emphasize similarities and differences. Those for Pd/PbS (Fig. 3) are very similar to those for Au/PbS and decompositions for Cr and Co spectra are not shown because visual inspection is sufficient to identify the relative amounts of the substrate and the adatom-induced components. More quantitative information about intensity variations is given through the attenuation curves of Figs. 6–8. These were determined by measuring the total integrated core-level emission after the deposition of θ Å of metal and normalizing that quantity to the emission for the cleaved surface, $\ln[I(\theta)/I(0)]$. In such attenuation curves, layer-by-layer metal growth would be revealed by a straight line with $1/e$ decay length corresponding to the photoelectron mean free path. In addition, the line-shape decomposi-

tions make it possible to determine the behavior of each of the components through component-specific attenuation curves, as shown in Figs. 6 and 7.

The results for the cleaved PbS(100) surface are shown at the bottom of Fig. 1. For the Pb $5d_{3/2,5/2}$ emission, the fitting parameters at $h\nu=60$ eV were spin-orbit splitting 2.60 eV, branching ratio 0.77, Gaussian width 0.47 eV, and Lorentzian width 0.20 eV. The corresponding results for S $2p_{1/2,3/2}$ at $h\nu=204$ eV were spin-orbit splitting 1.20 eV, branching ratio 0.50, Gaussian width 0.73 eV, and Lorentzian width 0.19 eV. We found no evidence for a surface-shifted component from the Pb $5d$ or S $2p$ data, consistent with the minimal relaxation and charge redistribution expected for the surface of a rock-salt structure. Our subsequent fits of the Pb $5d$ and S $2p$ substrate emission during interface formation were based on a single pair of spin-orbit-split Voigt functions. The absence of a surface-shifted component for PbS(100) is consistent with the results of Lai *et al.*⁵ for PbTe(100). They found that a surface-shifted component could im-

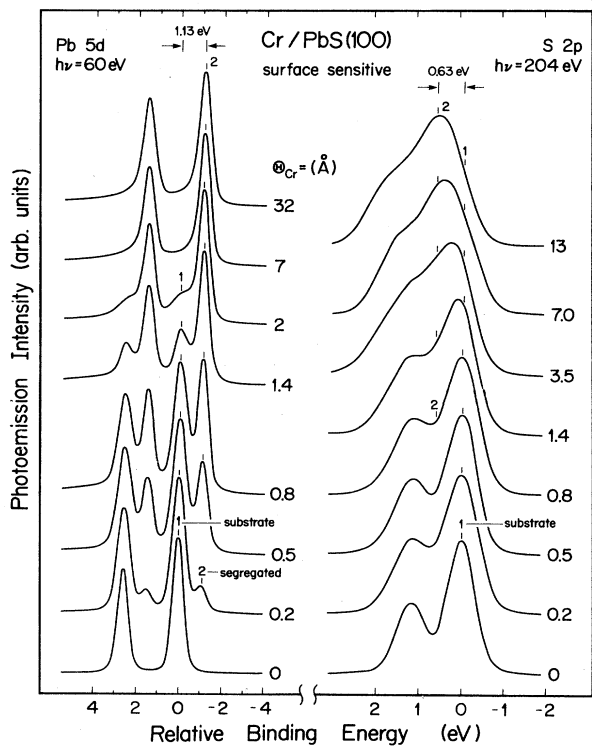


FIG. 1. Surface-sensitive Pb $5d$ and S $2p$ photoemission spectra as a function of Cr coverage. The spectra have been background subtracted, normalized, and corrected for band bending. The deposition of small amounts of Cr produces a new chemical configuration for both Pb and S. For Pb, the lower energy doublet persists to high coverage and corresponds to surface-segregated atoms. For S, there is likely to be a Cr-S reaction product as well as S outdiffusion into the overlayer. The width of the final component, labeled 2, indicates the presence of several inequivalent bonding configurations.

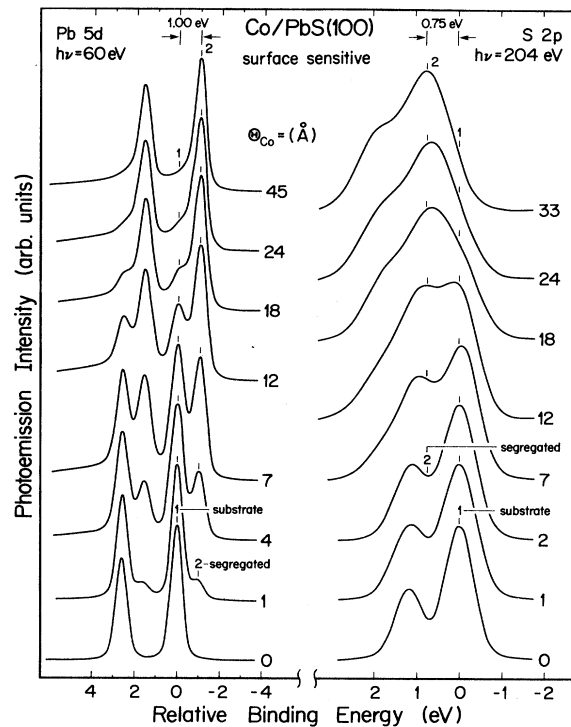


FIG. 2. Surface-sensitive Pb $5d$ and S $2p$ photoemission spectra as a function of Co deposition, analogous to those of Fig. 1.

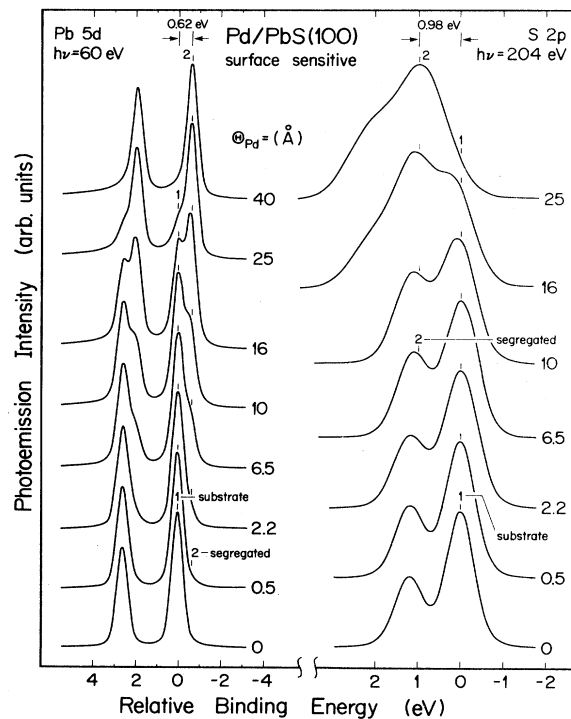


FIG. 3. Surface-sensitive Pb $5d$ and S $2p$ photoemission spectra as a function of Pd deposition, analogous to those of Fig. 1.

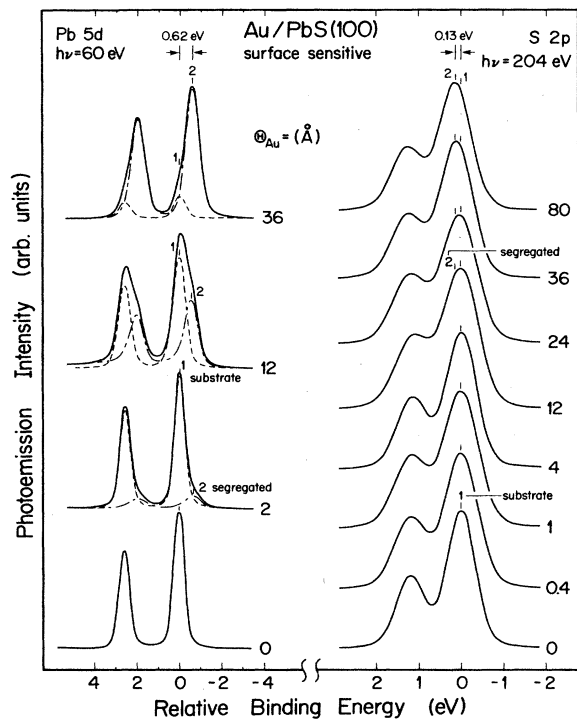


FIG. 4. Surface-sensitive Pb 5*d* and S 2*p* photoemission spectra as a function of Au deposition, analogous to those of Fig. 1.

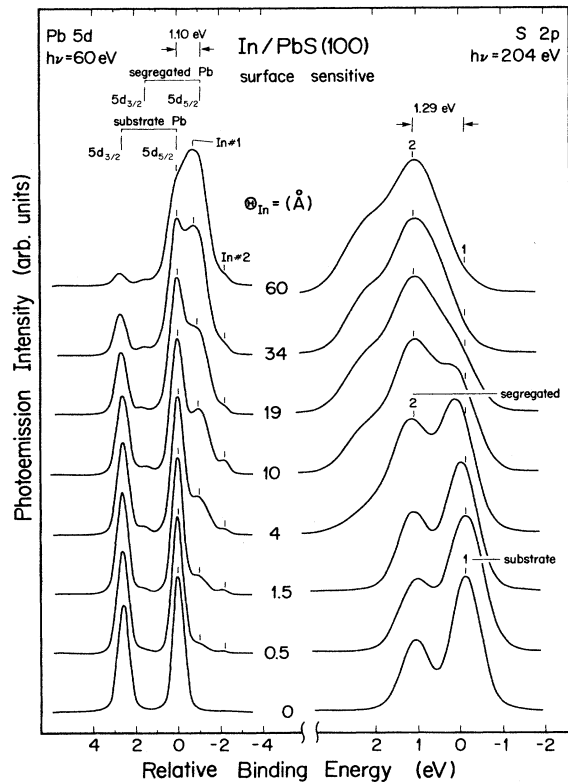


FIG. 5. Surface-sensitive Pb 5*d* and S 2*p* photoemission spectra as a function of In deposition, analogous to those Fig. 1. Notice that no significant free Pb signal is observed in these spectra.

prove their fits, but spectra collected at grazing angles did not show an increase in the surface component.

Lead behavior

The surface-sensitive Pb 5*d* core-level results summarized on the left-hand side of Figs. 1–4 show that adatoms of Cr, Co, Pd, and Au disrupt the substrate and that a new Pb 5*d* doublet appears on the low-binding-energy side of the substrate feature. As shown, this shifted component is readily apparent by coverages of 0.2 Å for Cr, 1 Å for Co, 2.2 Å for Pd, and 2 Å for Au. At higher coverages, it becomes a sharp, well-defined feature, and its *relative* intensity grows until it is the only one present at ~7 Å for Cr and 40–50 Å for Co, Pd, and Au. Such relative growth is a consequence of both substrate attenuation and the conversion of Pb atoms from the environ-

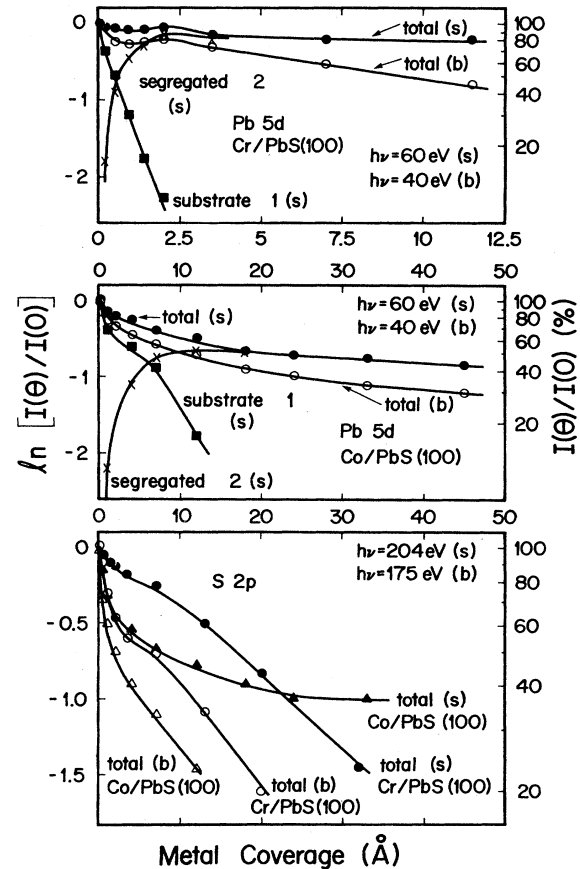


FIG. 6. Top and middle panels: Pb 5*d* attenuation curves for Cr/PbS(100) and Co/PbS(100). The component-specific attenuation results for the surface-sensitive spectra show the rapid decay of the substrate for Cr/PbS and the growth of the segregated component. Pb persists at high coverage because of its low solubility in Cr. The results for Co/PbS are analogous but the amount of disruption is much smaller. Bottom panel: S 2*p* core-level attenuation curves for Cr/PbS(100) and Co/PbS(100) at photon energies of 204 and 175 eV. For Cr/PbS, the bowing is due to the growth of the Cr-S reaction product and its subsequent attenuation.

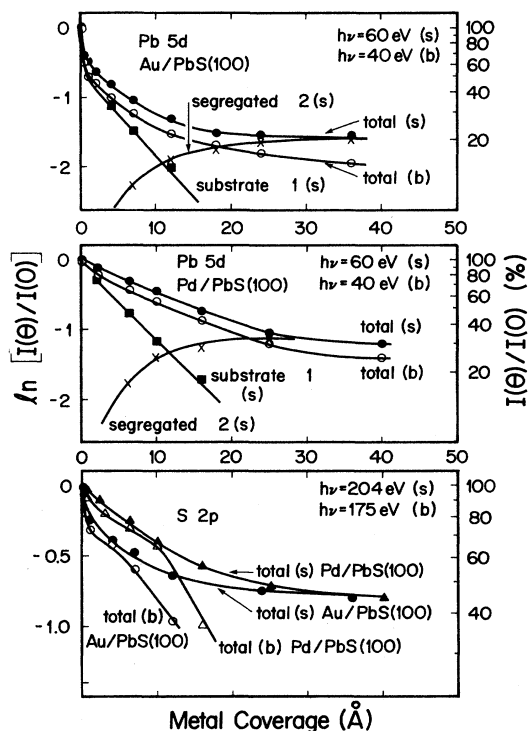


FIG. 7. Top and middle panels: Pb 5d attenuation curves for Au/PbS(100) and Pd/PbS(100) analogous to those of Fig. 6. Bottom panel: S 2p core-level attenuation curves for Au/PbS(100) and Pd/PbS(100) at photon energies of 204 and 175 eV.

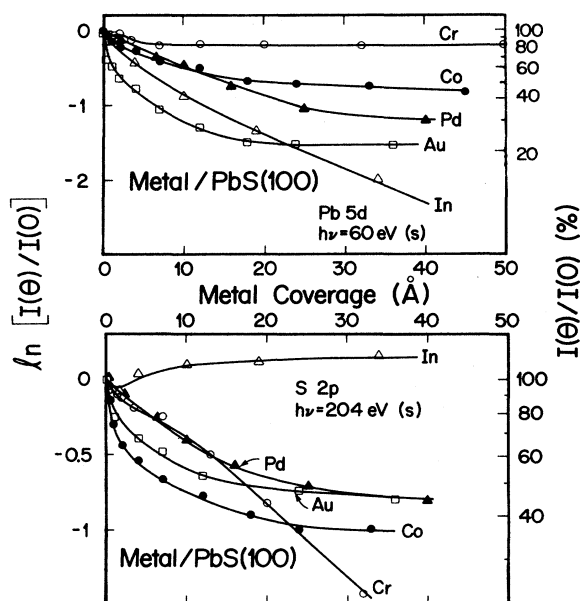


FIG. 8. Summary of attenuation curves for the total surface-sensitive Pb 5d and S 2p emission showing that the Pb expulsion is greatest for Cr and least for Au and that Pb is dissolved in the thickening In overlayer. For S, the trend is reversed with the greatest expulsion being observed for In overlayers and the least for Cr because of reaction with Cr.

ment of the substrate to that of a disrupted chemical configuration. Indeed, it is interesting to note the coverage at which the two components are equal, it being lowest for Cr (0.8 Å) and ~ 8 Å for Co, ~ 12 Å for Pd, and ~ 20 Å for Au. This indicates that ~ 0.8 Å of Cr is sufficiently disruptive that only half the emission is from those Pb atoms in Pb-S bonding configurations. The amount of substrate disruption can be estimated from the attenuation curves of Figs. 6 and 7. For Cr, the amount is roughly 9 Å. For the other overlayers, the amount of disruption is considerably less.

The Gaussian width of the disrupted-Pb component is well defined at low coverages (e.g., FWHM of 0.43 eV for 2 Å of Cr), and this indicates that Pb is found in a relatively uniform chemical environment. (Alternatively, it could indicate that Pb is insensitive to that environment, but the results of Figs. 1–4 show Pb 5d shifts of 0.62–1.13 eV for these metals.) With increasing metal deposition, the disrupted-Pb 5d core-level component showed only slight variations in the Gaussian width (0.43–0.41 eV for Cr between 1 and 13 Å), remaining sharp and well defined at higher coverages. Spectra at intermediate coverages can be fit with weighted amounts of the substrate, and the shifted components appear at the same position for all coverages (lower binding energy relative to the substrate of $1.13 \text{ eV} \pm 0.03 \text{ eV}$ for Cr, $1.00 \text{ eV} \pm 0.03 \text{ eV}$ for Co, and $0.62 \text{ eV} \pm 0.03 \text{ eV}$ for Au and Pd relative to the substrate). For the shifted component, it was necessary to use the DS line shape because of metallic screening for Pb atoms released in the metallic overlayer (DS asymmetry factors of 0.12 for Cr, 0.11 for Co, Au, and Pd).

The results shown in Figs. 1–4 show the disappearance of the substrate component and the growth of a disrupted component at a fixed energy relative to the substrate. This is shown quantitatively for Cr/PbS at the top of Fig. 6 where there is a rapid decrease in the substrate component (labeled 1) as a function of Cr deposition but a rapid increase in the disrupted component (labeled 2). For the surface sensitive results (s), the total amount of Pb present decreases only slightly relative to the cleaved surface so that by a deposition of 10 Å the amount of Pb emission is 80% of that of the starting surface. The bulk-sensitive results show a smaller Pb contribution, again normalized to the clean surface emission. Together, these results indicate Pb enrichment of the surface region. In particular, Pb atoms released from the PbS substrate by the deposition of Cr are expelled from the growing Cr overlayer and segregate to the surface. At high coverage, the amount of Pb at the surface remains almost unchanged, as can be seen from the almost flat Pb 5d attenuation curve at the top of Fig. 8.

Analogous behavior is exhibited for Co/PbS, but the rate at which the substrate is converted and/or covered up is slower, and the overall amount of surface-segregated Pb is smaller (center panel of Fig. 6 and top of Fig. 8). For Pd and Au, these rates are reduced further. From the top panel of Fig. 8, were the Pb surface sensitive attenuation curves are compared, we can see that the amount of Pb present in the surface region is greatest for Cr and then decreases in the order Co, Pd, Au (see espe-

cially the results after 40 Å deposition because the substrate component is completely attenuated). The constant shift in binding energy of the Pb 5*d* component and the small variation in Gaussian width with coverage are indications that the segregated Pb atoms are in reasonably equivalent chemical environments. Moreover, the persistence of the liberated atoms at the surface indicates that they are very slowly incorporated in the thickening layer (dissolved or kinetically trapped). This is consistent with the estimated positive heats of solution of Pb in Cr, Co, and Au (136.7, 97.2, 10.4 kJ/mole, respectively).²⁸ For Pd, the heat of solution would indicate a more favorable mix, -89 kJ/mole, but the experimental results indicate that Pd and Au behave in analogous fashions.

It is interesting to point out that the relative binding energy of the segregated Pd 5*d* component is identical for Au and Pd overlayers and relatively close for Co and Cr overlayers. The changes in relative binding energy can be related to differences in chemical environments for these segregated atoms. If we assume that the Pb atoms are coordinated with only metal atoms, then their energies should track with their heats of solution in those metals. Indeed, our results show a larger shift for the reactive metals than for the less reactive metals, in agreement with the heats of solution. The fact that (Cr, Co) and (Pd, Au) show similar shifts indicates the qualitative character of this correlation and the fact that the segregated atoms are not fully coordinated in a three-dimensional sense. Analogous trends and qualitative agreement with solubilities have been reported for metal-GaAs and metal-InP interfaces where the final energy position of the cations corresponds to the dilute limit.²⁹

Comparison of these metal-PbS interface results to those for metal-InP and -GaAs interfaces show both similarities and differences as far as the cation behavior is concerned. For PbS, the constant binding energy of the Pb 5*d* core levels suggests chemical environments which are relatively constant, consistent with a model in which the Pb atoms are strongly expelled to the surface. In contrast, the Ga emission at disrupted interfaces always shifts steadily to lower binding energy, indicating that the Ga atoms released from the substrate and detected in the photoemission experiments are in progressively higher dilution in the metal overlayer.³⁰⁻³³ Although Ga segregation is observed, it is not detected at high coverage for overlayers of Cr, Co, and Pd. Ga does persist at the surface for Au overlayers. For In released at the corresponding metal-InP interfaces, we find strong expulsion. At high coverage, there is a shift in In 4*d* binding energy when the In content of the surface region starts to diminish. Indium at the Cr- and Co-based InP interfaces then behaves in an analogous fashion to Pb except that the In solubility in the overlayer is higher. For the Pd/InP and Au/InP interfaces, the behavior is quite different because of the expulsion of P and the more effective retention of In in the metal layer due to the more favorable Pd-In and Au-In bonds.

In a recent paper we examined segregation at a large number of metal-semiconductor interfaces, showing that the effect can be qualitatively understood in terms of a model which considers the cohesive energy and relative

atomic sizes of the substrate and overlayers species.^{29,34} Following Ref. 34, the cohesive energy of Pb is lower than that of Ga or In, and the atomic size of Pb is larger than Ga or In. The model then predicts that Pb would be expelled to the surface of a given metal overlayer more readily than would either Ga or In, consistent with the above discussion. Indeed, the Pb 5*d* attenuation curves of Figs. 6-8 show substantial Pb at the surface and little tendency to be dissolved at high metal coverages.

The In/PbS(100) interface evolves differently from those discussed above. As shown in Fig. 5, the deposition of In produces a weak Pb 5*d* component at 1.10 eV ± 0.03 eV lower binding energy. This can best be seen from the Pb 5*d*_{3/2} component of Fig. 5 because of the overlap of the Pb 5*d*_{5/2} component with the growing In 4*d* emission (labeled 1 and 2). Whereas this adatom-induced component does grow, it remains small compared to the substrate emission. Even after the deposition of 34 and 60 Å of In, it is considerably weaker than the substrate component, and we conclude that the released Pb atoms are not expelled as strongly to the surface. This is consistent with the thermodynamic heat of solution of Pb in In, namely -296 kJ/mole.²⁸ Moreover, the spectra of Fig. 5 and the attenuation results of Fig. 8 show that the substrate is still visible after ~60 Å. At that coverage, the 1/*e* decay length of 22 Å is much too large for layer-by-layer growth. We conclude that there is In adatom clustering on the surface, analogous to what has been reported for In/PbTe³⁻⁵ and other semiconductor surfaces.^{35,36} Finally, it is interesting to note that there is a small feature shifted to lower binding energy relative to the dominant In emission (labeled In 2 in Fig. 5). We associate this with In atoms coordinated with Pb, consistent with the small amount of Pb that is in an environment different from PbS.

Cross sectional slices through these fully developed interfaces (except In) would show a concentration of Pb atoms near the surface, limited amounts of Pb in solution, and relatively little at the buried interface. The amount of Pb present at the surface would be greatest for Cr (where the solubility is lowest) and lowest for Au or Pd. The growth mode appears to be uniform layer by layer. In contrast, In adatoms exhibit a strong tendency for clustering. For In/PbS, it is likely that there will be Pb near the buried interface because of its solubility in indium.

Sulfur behavior

These generalizations concerning the distribution of Pb atoms can be only partially extended to the S atoms. Similarities are reflected in adatom-induced S 2*p* core-level component, as shown at the right of Figs. 1-5, while differences involve the origin of the reacted component.

On the right-hand side of Fig. 1, we present background-subtracted surface-sensitive S 2*p* core-level EDC's for Cr/PbS(100) taken at a photon energy of 204 eV. Small amounts of Cr disrupt the substrate, as shown at the left of Fig. 1 for Pb, and there are changes in the S spectra reflected by a broadening of the core-level emission (Gaussian width 740-840 meV for 0.2-1.4 Å com-

pared to 730 meV for the clean surface). With increasing deposition, the S 2*p* centroid shifts to higher binding energy as the Cr-induced component grows and the substrate contribution is attenuated. Comparison with the Pb attenuation results of Fig. 6 shows that the substrate contribution is negligible after the deposition of ~ 5 Å of Cr. At 13 Å deposition, the new component appears at 0.63 ± 0.03 eV relative to the substrate. Even at this coverage, however, it is very broad, indicating a variety of inequivalent chemical configurations. At higher coverage, the Cr-induced component narrowed slightly.

At the bottom of Fig. 6, we show changes in the integrated S 2*p* emission as a function of Cr coverage for photon energies of 175 (open circles) and 204 eV (closed circles). The surface-sensitive data taken at $h\nu = 204$ eV reveal the slow decrease in the S 2*p* intensity for the first few angstroms of deposition, a slower rate until ~ 10 Å, and then a rate which corresponds to a $1/e$ length of ~ 20 Å (compared to a photoelectron mean free path of 4 Å). The data taken with a higher escape depth ($h\nu = 175$ eV, $\lambda \sim 9$ Å) show a much more rapid decay, the inflection, and then a $1/e$ decay length of ~ 14 Å. From the Pb spectra with its well-separated components, we can estimate the amount of disruption to be ~ 9 Å and again note that the substrate $1/e$ length is less than 1 Å while disruption is occurring. The attenuation curves therefore represent the rapid loss of emission from the retreating substrate, the growth of the reacted component, and then the gradual reduction in S emission with increasing Cr deposition. Moreover, these results show that the amount of S near the surface is greater than that farther from the surface at higher coverage, indicating significant surface segregation of S. The inequivalent chemical environments are reflected by the broad S 2*p* core-level emission of Fig. 1. The formation of a Cr-S reaction product is also consistent with the heats of formation of bulk Cr-S compounds (e.g., CrS at -155 kJ/mole and Cr₂S₃ at -364 kJ/mole).³⁷ Comparing the results at the top and bottom of Fig. 8 for Cr/PbS shows that the amount of Pb segregation is much greater than that of S and that this interface represents the extreme case for adatom-induced reaction and anion trapping.

The Co/PbS(100) interface also provides evidence of a new S component shifted 0.75 ± 0.03 eV with substantial broadening at low coverage. Examination of the EDC's indicates that changes occur much more slowly for Co/PbS than for Cr/PbS. (A similar conclusion can be drawn from the Pb spectra by noting the amount of metal which is needed to produce two pairs of doublets of equal intensity.) In particular, these S results indicate that the amount of metal sulfide which forms is very small and may be negligible. Indeed, a better description of interface evolution would be based on the Co/GaAs system where limited disruption was observed, where As was both dissolved in the overlayer and segregated, and where no compounds were formed.³⁸ The heats of formation for Co-S are favorable, but to a lesser extent than Cr.³⁷

The results for the Pd/PbS(100) and In/PbS(100) systems also indicate limited disruption and the formation of a readily distinguishable new bonding configuration for S (0.98 ± 0.03 eV for Pd and 1.29 ± 0.03 eV for In relative to

the substrate). For Au/PbS(100), the S 2*p* core-level spectra show a slight shift toward higher binding energy at high metal coverages for the Au-induced component, labeled 2 in Fig. 4. Indeed, it is difficult to separate the two components. As for Co, the heats of formation for Pd-S, Au-S, and In-S compounds are low and the interface profile can be described in terms of segregation and solution rather than compound formation.³⁷

Finally, we note from Fig. 8 that the amount of segregated Pb and S at high coverage is comparable for Co/PbS and Pd/PbS with Pb segregation being the stronger for Co/PbS and S segregation being stronger for Pd/PbS. For Au/PbS, the amount of S segregation is much greater than Pb. For In/PbS, the solubility of S in In is so low that the S emission at high coverage actually exceeds that observed for the cleaved, clean surface. For In/PbS, the minimum observed at low coverage in the attenuation curve for S is analogous to that encountered for InP interfaces; it is related to the growth of In nuclei of sufficient size that expulsion of the S is energetically favored. Again from Fig. 8, the Cr/PbS and In/PbS interfaces appear as the extremes with symmetric behaviors for Pb and S observed in these two systems. It is quite

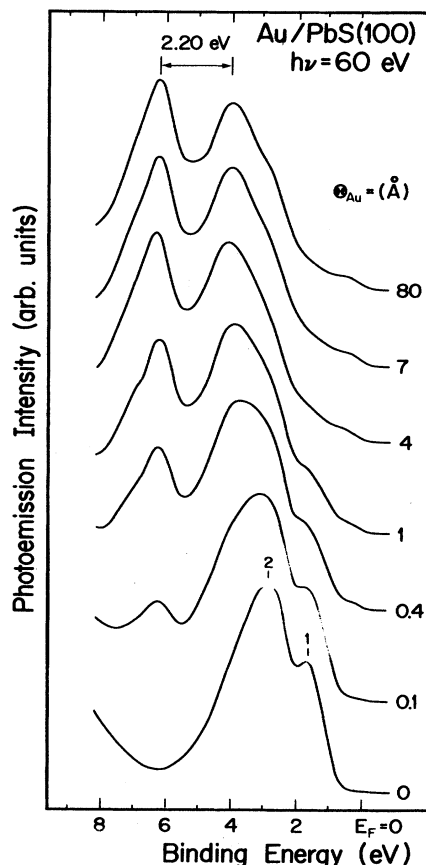


FIG. 9. Valence-band energy distribution curves for Au/PbS as measured with a photon energy of 60 eV showing the failure of the overlayer to converge to that representative of pure Au.

clear that the EDC's and the attenuation curves reflect the balance between reaction, solubility, and segregation at high coverage and that the chemical driving forces are equivalent for these thin films.

The results obtained with core-level photoemission for Au/PbS(100) interface are complemented by valence-band results, as shown in Fig. 9 for spectra taken with a photon energy of 60 eV. Peaks labeled 1 and 2 in the bottom-most EDC are due to the three S-derived $3p$ -type valence bands of PbS and agree well with the previously XPS and UPS spectra.^{19–21} The s -type bands derived from Pb $6s$ levels are located ~ 8 eV below the Fermi level and are not shown in our spectra. The deposition of Au leads to the development of states at the Fermi level. These states are apparent at 0.4 Å and are typical for a metallic interface surface layer. The very strong Au $5d$ emission can easily be seen for coverages as low as 0.1 Å. By ~ 1 Å, the Au $5d$ splitting is ~ 2.2 eV and remains constant for higher Au coverages. This value is smaller than the value for bulk Au (2.4 eV), but is close to that reported for Au/Ge interfaces.³⁹ As for Au/Ge, we conclude the presence of S and to a lesser extent Pb in the surface region to be responsible for the deviation from the pure-Au splitting.

Schottky barrier formation

The detailed line-shape analysis for the Pb $5d$ spectra makes it straightforward to determine changes in substrate core-level binding energies as a function of metal deposition and thereby investigate Schottky barrier formation. For the clean surface, we found the Fermi level to lie almost at the conduction-band minimum. From the Pb $5d$ spectra of Figs. 1–5, we measured total changes in Fermi level position of -0.15 ± 0.02 eV for Cr/PbS, -0.09 ± 0.02 eV for Co/PbS, -0.13 ± 0.02 eV for In/PbS, 0.10 ± 0.02 eV for Au/PbS, and 0.16 ± 0.02 eV for Pd/PbS, where negative values indicate movement of the Fermi level into the conduction band. The final pin-

ning positions for Cr, Co, and In correspond to degenerate positions of the Fermi level above the bottom of the conduction band. Contrary behavior is observed for Au and Pd, where the measured final positions of the Fermi level are within the band gap. These results are similar to those reported in Refs. 3–5, where degenerate Fermi level positions were found for p -PbTe(100) for the materials Pb, Al, Ge, and In and where Au deposition led to a final pinning position within the band gap. A general observation is that the final position of the Fermi level is fixed at submonolayer coverages for all interfaces and varies considerably depending on the metal deposited to form the overlayer.

CONCLUSIONS

These core-level photoemission results have allowed us to describe the evolution of the metal-PbS(100) interface for the representative metals Cr, Co, Pd, Au, and In. In all cases, the deposition of metal atoms triggers substrate disruption and the formation of interfaces which are not atomically abrupt. Instead, there is out-diffusion of both Pb and S atoms. Surface segregation is observed for these released atoms with an amount determined by the solubility in the evolving metal layer (this solubility changes as the layer thickens, as discussed for metal III-V interfaces).

ACKNOWLEDGMENTS

This work was supported by the National Science Foundation under Grant No. DMR 86-10837. The photoemission experiments were conducted at the Wisconsin Synchrotron Radiation Center, which is supported by the National Science Foundation, and the support of the personnel of that facility is gratefully acknowledged. Data analysis was greatly facilitated by access to IBM PC/RT's provided through an IBM Materials Science and Processing Grant.

¹See the following for reviews of photoemission results for a variety of metal-semiconductor interfaces: D. M. Hill, F. Xu, Z. Lin, and J. H. Weaver, *Phys. Rev. B* **38**, 1893 (1988). L. J. Brillson, *Surf. Sci. Rep.* **2**, 123 (1982); W. E. Spicer, T. Kendelewicz, N. Newman, K. K. Chin, and I. Lindau, *Surf. Sci.* **168**, 240 (1986); R. H. Williams, in *Physics and Chemistry of III-V Compound Semiconductor Interfaces*, edited by C. W. Wilmsen (Plenum, New York, 1985); R. Ludeke, *Surf. Sci.* **168**, 291 (1986).

²For a good review of the information gained by techniques other than photoemission (which are emphasized herein), see L. C. Feldman and J. W. Mayer, *Fundamentals of Surface and Thin Film Analysis* (North-Holland, New York, 1986).

³F. Cerrina, R. R. Daniels, and V. Fano, *Appl. Phys. Lett.* **43**, 182 (1983).

⁴F. Cerrina, R. R. Daniels, and Te-Xiu Zhao, *J. Vac. Sci. Technol. B* **1**, 570 (1983).

⁵B. Lai, G. M. Wells, F. Cerrina, J. R. Anderson, L. Papagno,

and G. J. Lapeyre, *J. Vac. Sci. Technol. A* **4**, 977 (1986).

⁶N. K. Abriksov, V. V. Bankina, L. V. Poretskaya, L. E. Shelimova, and E. V. Skudnova, *Semiconducting II-VI, IV-VI, and V-VI Compounds* (Plenum, New York, 1969).

⁷Y. I. Ravich, B. A. Efimova, and J. A. Smirnov, *Semiconducting Lead Chalcogenides* (Plenum, New York, 1970).

⁸H. Prier, *Appl. Phys.* **20**, 189 (1979).

⁹W. Lo and F. E. Gifford, *J. Electrochem. Soc.* **127**, 1372 (1980).

¹⁰D. E. Swets and C. R. Harrington, *J. Electrochem. Soc.* **131**, 172 (1984).

¹¹F. Herman, R. L. Kortum, I. Ortenburger, and J. P. Van Dyke, *J. Phys. (Paris) Colloq.* **29**, C4 (1968).

¹²L. E. Johnson, J. B. Conklin, Jr. and G. W. Pratt, Jr., *Phys. Rev. Lett.* **11**, 538 (1963); J. B. Conklin, Jr., L. E. Johnson, and G. W. Pratt, Jr., *Phys. Rev.* **137**, A1283 (1965).

¹³S. Rabii, *Phys. Rev.* **167**, 801 (1968).

¹⁴H. Overhof and U. Rössler, *Phys. Status Solidi B* **37**, 691 (1970).

- ¹⁵S. E. Kohn, P. Y. Yu, Y. Petroff, Y. R. Shen, Y. Tsang, and M. L. Cohen, *Phys. Rev. B* **8**, 1477 (1973).
- ¹⁶P. J. Lin and L. Kleinman, *Phys. Rev.* **142**, 478 (1966).
- ¹⁷Y. W. Tung and M. L. Cohen, *Phys. Rev.* **180**, 823 (1969).
- ¹⁸G. Martinez, M. Schlüter, and M. L. Cohen, *Phys. Rev. B* **11**, 651 (1975).
- ¹⁹F. R. McFeely, S. Kowalczyk, L. Ley, R. A. Pollak, and D. A. Shirley, *Phys. Rev. B* **7**, 5228 (1973).
- ²⁰T. Grandke, L. Ley, and M. Cardona, *Phys. Rev. Lett.* **38**, 1033 (1977).
- ²¹T. Grandke, L. Ley, and M. Cardona, *Phys. Rev. B* **18**, 3847 (1978).
- ²²T. Grandke and M. Cardona, *Surf. Sci.* **92**, 385 (1980).
- ²³M. H. B. Stiddard, *Thin Solid Films* **82**, 337 (1981).
- ²⁴F. Xu, C. M. Aldao, I. M. Vitomirov, Z. Lin, and J. H. Weaver, *Phys. Rev. B* **36**, 3495 (1987).
- ²⁵G. K. Wertheim and S. B. DiCenzo, *J. Electron Spectrosc. Relat. Phenom.* **37**, 57 (1985).
- ²⁶S. Doniach and M. Šunjić, *J. Phys. C* **3**, 285 (1970).
- ²⁷J. J. Joyce, M. del Giudice, and J. H. Weaver, *J. Electron Spectrosc. Relat. Phenom.* (to be published) provides a detailed discussion of our line-shape analysis procedure.
- ²⁸A. K. Niesen, F. R. Deboer, R. Boom, P. F. de Chatel, W. C. M. Mattens, and A. C. Miedema, *CALPHAD* **7**, 51 (1983).
- ²⁹Z. Lin, F. Xu, and J. H. Weaver, *Phys. Rev. B* **36**, 5777 (1987).
- ³⁰T. Kendelewicz, R. S. List, K. A. Bertness, M. D. Williams, I. Landau, and W. E. Spicer, *J. Vac. Sci. Technol. B* **4**, 959 (1986); T. Kendelewicz, W. G. Pedro, I. Lindau, and W. E. Spicer, *J. Vac. Sci. Technol. A* **2**, 542 (1984); *Phys. Rev. B* **28**, 3618 (1983).
- ³¹R. Ludeke and G. Landgren, *Phys. Rev. B* **33**, 5526 (1986).
- ³²C. M. Aldao, I. M. Vitomirov, F. Xu, and J. H. Weaver, *Phys. Rev. B* **37**, 6019 (1988).
- ³³I. M. Vitomirov, C. M. Aldao, Z. Lin, Y. Gao, B. M. Trafas, and J. H. Weaver, *Phys. Rev. B* **38**, 10 776 (1988).
- ³⁴J. H. Weaver, Z. Lin, and F. Xu, in *Surface Segregation and Related Phenomena*, edited by P. A. Dowben and A. Miller (CRC, Boca Raton, in press), Chap. 10.
- ³⁵D. E. Savage and M. G. Lagally, *Phys. Rev. Lett.* **55**, 959 (1985).
- ³⁶I. M. Vitomirov, C. M. Aldao, B. M. Trafas, J. J. Joyce, and J. H. Weaver, unpublished results for In/Si, In/GaAs, In/InP, and In/InSb.
- ³⁷NBS Tables of Chemical Thermodynamical Properties [*J. Phys. Chem. Ref. Data* **11**, Suppl. 2 (1982)]; O. Kubachewski and C. B. Alcock, *Metallurgical Thermochemistry* (Pergamon, Oxford, 1979).
- ³⁸F. Xu, J. J. Joyce, M. W. Ruckman, H.-W. Chen, F. Boscherini, D. M. Hill, S. A. Chambers, and J. H. Weaver, *Phys. Rev. B* **35**, 2375 (1987).
- ³⁹M. W. Ruckman, J. J. Joyce, F. Boscherini, and J. H. Weaver, *Phys. Rev. B* **34**, 5118 (1986).